

The Promotion of Particulate Matter Oxidation by Oxide Ion Conductors, Zr–Y–O and Zr–Nd–O

Koichiro Harada,* Hiroshi Yamada, and Akihide Takami

Mazda Motor Corporation, 3-1 Shinchi, Fuchu-cho, Aki-gun, Hiroshima 730-8670

Received August 22, 2011; E-mail: harada.koui@mazda.co.jp

Catalytic particulate matter oxidation and its promotion by high oxide ion conductors, Zr–Y–O and Zr–Nd–O, has been studied. Zr-Based oxides show higher particulate matter oxidation activity by O_2 compared to a Ce-based conventional catalyst using Pt-loaded oxide coated on a DPF substrate. Isotopic tracer methods involving ^{18}O indicate Zr-based oxides release a large amount of lattice oxygen during carbon oxidation. Also, unique to the Zr-based oxides is an electron and electromotive force generation between carbon-deposited sites and carbon-free sites during carbon oxidation. Zr-Based oxides appear to have the capability to effectively generate oxide ions well suited for carbon oxidation.

Diesel engines are widely used because of their superior fuel economy, high torque, and high durability. Recently, they have been receiving increased attention due to their ability to help address global warming by reducing CO_2 emissions. However, reducing the emission of other potentially harmful compounds such as particulate matter (PM) and nitrogen oxides (NO_X) continues to be an issue[1,2] as various countries introduce stricter emission regulations. The use of a diesel particulate filter (DPF) in a vehicle's after-treatment system is one of the most promising technical solutions being used to reduce PM emissions.[3,4] A DPF has a finite capacity for PM, and as PM loading builds, DPF backpressure increases and reduces engine power and fuel economy. The DPF needs to be periodically "regenerated," and PM has to be burned off by raising the exhaust gas temperature to a level high enough to oxidize the PM with O_2 (typically $\approx$600 °C). This DPF "regeneration" temperature is higher than that found during normal diesel engine operation and requires special engine tuning and increased fuel consumption to obtain. It is possible to attain lower temperature PM oxidation with NO_2 or SO_2.[5–7] However, recent combustion technology improvements of diesel engines such as PCCI (premixed charge compression ignition) have resulted in lowering NO_X components in the exhaust gas. SO_X concentration in the exhaust gas has also been reduced as a result of lower sulfur content in diesel fuels. Thus, DPF regeneration independent of NO_2 or SO_2 is becoming necessary.

DPF regeneration typically involves post injection of excess diesel fuel across a diesel oxidation catalyst placed upstream of the DPF. The injected fuel creates an exotherm at the catalyst and raises the exhaust gas temperature at DPF inlet. This excess fuel injection results in poorer fuel economy. Fuel economy can be improved by reducing the temperature and/or duration of the DPF regeneration event. Catalyzed DPFs have been investigated intensively to promote the oxidation reaction of PM, lower regeneration temperature, and improve fuel economy.

For over a decade, catalytic PM oxidation on a wall-flow type DPF has been examined, and various studies of catalyst materials to enhance the PM oxidation performance have been performed. For example, catalysts incorporating alkali metals and alkali earth metals have proven to decrease PM oxidation temperature.[8] However, use of alkali metals in such catalysts is limited due to poor thermal durability above 800 °C.

Ce-Based oxides are well known as PM oxidation catalysts,[9–12] and several studies on promoting schemes have been reported. These studies indicate that lattice oxygen released from the surface of the Ce-based oxides promotes the oxidation of PM. Some of the previous studies have shown the importance of the oxygen exchange reaction in low-temperature PM oxidation via isotopic tracer methods.[13–15] In the oxygen exchange reaction, dissociative adsorption of gas phase oxygen and desorption of the oxygen from the oxide occur simultaneously. This results in effective and continuous supply of active oxygen to PM from the oxide. However the PM oxidation performance of Ce-based oxides strongly depends on surface lattice oxygen.[16] Therefore, surface area reduction by thermal aging lowers the activity of the oxygen exchange reaction and a leads to a deterioration of the PM oxidation performance.

The objective of this study is to achieve a high, thermally-resistive, PM oxidation catalytic activity with O_2. For this purpose, we employed a promoting scheme to supply bulk lattice oxygen and prevent catalytic deterioration caused by surface area reduction. An effective way to supply bulk lattice oxygen is through mobility enhancement of the bulk oxide ion to the surface of the oxide. Based on this assumption, oxide ion conductors have been studied as potential materials to enhance the supply of active oxygen both from surface and oxide bulk. This paper describes the catalytic activities of PM oxidation using two Zr-based oxides with high oxide ion conductivity, Zr–Y–O and Zr–Nd–O. Also presented are characterization results to investigate the PM oxidation mechanism of the Zr-based oxides by means of an isotopic tracer method and electrochemical measurement.

Published on the web December 6, 2011; doi:10.1246/bcsj.20110250

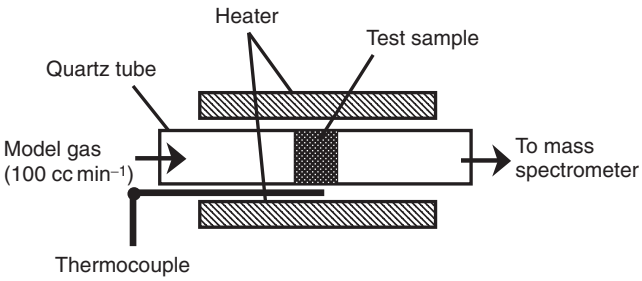

Figure 1. Simplified schematic of the redox property measurement.

Experimental

Catalyst Preparation and Characterization. $Zr_{0.8}Y_{0.2}O_{2-X}$ (ZrYO) and $Zr_{0.7}Nd_{0.3}O_{2-X}$ (ZrNdO) were used as oxide ion conductors. While the molar ratios of Zr and the additive element in each of these two oxides are different, the molar ratios were selected to provide the highest carbon oxidation activity. For comparison, $Ce_{0.7}Zr_{0.3}O_{2-X}$ (CeZrO) was used as a conventional oxide possessing high oxygen storage capacity (OSC) and high thermal stability. ZrYO, ZrNdO, and CeZrO were prepared by a coprecipitation method using nitric acid of each rare earth metal. These precipitates were calcined in air at 500 °C for 2 h.

4.0 wt % Pt-containing catalysts were prepared by evaporation to dryness with a diamminedinitritoplatinum(II) nitrate solution. The thermal aging was performed in air at 800 °C for 24 h or 1000 °C for 24 h to simulate the thermal load by DPF regeneration in the real-world driving condition.

Structural features of the oxides were characterized by X-ray diffraction (XRD). XRD patterns were recorded with a Rigaku X-ray diffractometer (RINT2000) operated at 50 kV and 240 mA using Cu Kα radiation. Average crystalline diameters of oxides were determined from the full width at the half maximum of the X-ray diffraction peak with the Scherrer equation.

The BET surface areas of oxides were determined by physical adsorption of N_2 at −196 °C in a Shimadzu Micromeritics (FlowSorbII2300).

The redox properties of catalysts were observed by means of temperature-programmed H_2 reduction method (H_2-TPR) in a quartz reactor (inner diameter: 4 mm). Catalysts in aged condition were granulated and 100 mg of the catalysts were installed into a quartz tube shown in Figure 1. The catalysts were heated in 10% O_2 in He from room temperature to 600 °C as a pretreatment. After cooling to room temperature, the catalysts were heated to 600 °C again in 2% H_2 in He flow. The H_2O concentration under this heating process was measured by a quadrupole mass spectroscopy (ANELVA, AQA-100R). Because oxygen is purged and replaced with inert gas containing H_2, stored oxygen from within the catalyst is the only source available to oxidize the H_2. The amount of released oxygen is estimated from amount H_2O generated.

Catalytic Activity. Catalytic PM oxidation was studied in a TG/DTA (Seiko Instruments Co., Ltd., EXSTAR6000). Test samples contained a mixture of catalyst and carbon (carbon black, Sigma-Aldrich Corp., as an alternative to PM) and were

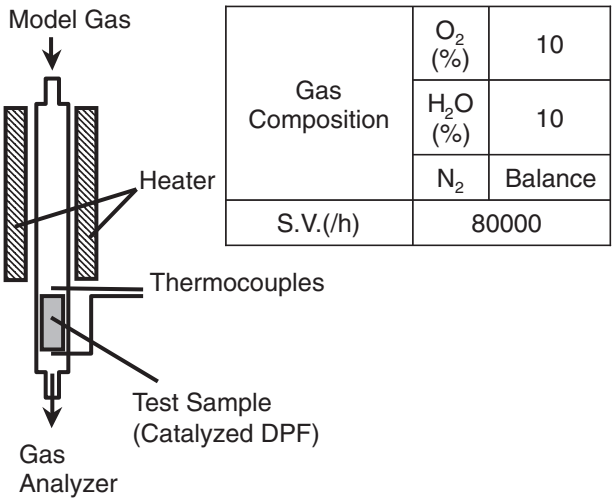

Figure 2. Simplified schematic of the synthesized gas analysis of catalytic carbon oxidation activity.

prepared by the following procedure. The thermally aged catalyst and carbon were mixed in the weight ratio of 4 to 1 and shaken by hand or sonication for 5 min to create a loose contact condition or tight contact condition, respectively. The mixture was placed into the sample crucible and heated from 50 to 800 °C at a heating rate of 10 °C min^{-1}. Gas composition was controlled at 10% O_2 in N_2. Differential thermal gravidity (DTG) was used to provide an index of the carbon oxidation rate of the catalysts.

Catalytic PM oxidation was also studied with catalysts loaded on a DPF substrate. The Pt-loaded catalysts were coated on a SiC-based DPF at 20 g per liter DPF volume. The catalyzed DPF (CDPF) was thermally aged in air at 800 or 1000 °C for 24 h. Carbon was loaded on the CDPF at 10 g per liter CDPF volume, and the CDPF was placed in a fixed-bed flow reactor as shown in Figure 2. Inlet gas temperature of the CDPF was heated from 100 to 600 °C at a heating rate of 10 °C min^{-1} under the gas conditions shown in the inset of the Figure 2. Carbon oxidation rate was determined by measuring the concentrations of CO_2 and CO generated.

Isotopic tracer studies were carried out in the quartz reactor mentioned above in the redox measurement. Oxygen isotope, ^{18}O, was used as a tracer to verify the oxygen source[17–19] in the carbon oxidation reaction. A mixture of 5 mg carbon black, 20 mg thermally aged catalyst and 100 mg SiC under the loose contact condition was prepared. The mixture was heated up to 600 °C in He gas (100 mL min^{-1}) and then the gas flow was switched to 3.5% $^{18}O_2$ in He (100 mL min^{-1}). In this experiment, CO_2 species ($C^{18}O^{18}O$, $C^{16}O^{18}O$, and $C^{16}O^{16}O$) and CO species ($C^{18}O$ and $C^{16}O$) were generated and distinctively measured by mass spectroscopy. Since oxygen in the gas phase was replaced with oxygen isotope, $^{18}O_2$, detected ^{16}O is identified as evolved oxygen from the catalyst.

Isotopic tracer experiments were also run without carbon (catalyst only). Each concentration of $^{18}O^{18}O$, $^{16}O^{18}O$, and $^{16}O^{16}O$ was measured with mass spectroscopy.

Electrochemical behavior of the catalysis on the carbon oxidation was studied. Experimental setup is shown in Figure 3. The purpose of this measurement is to characterize

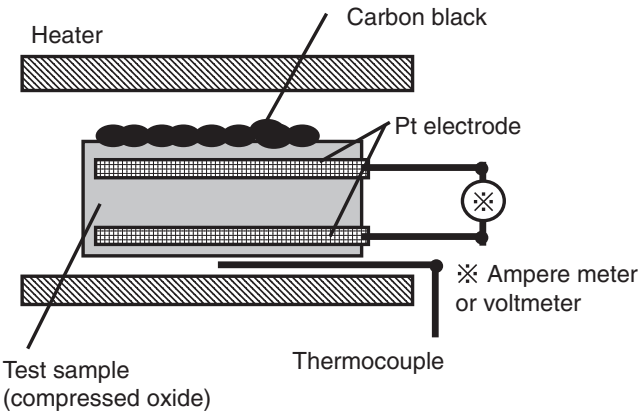

Figure 3. Simplified schematic of the in situ electrochemical observation of catalytic carbon oxidation [oxide pellet: 10 mm × 10 mm × 1.0 mm, Pt mesh: 25 mm^2 (80 meshes/cm^2)].

the behavior of lattice oxygen diffusion and electron transfer at the moment of carbon oxidation. Changes in the density gradient of the lattice oxygen as a result of carbon oxidation can be detected by electromotive force observations. In addition, electrons transferred during carbon oxidation generate electrical current and can be measured using an ampere meter. Because the electron conductivity of each oxide is much lower than the Pt electrode of the ampere meter, transferred electrons can be detected as a current.

Samples were prepared by the following procedure. A load of 1.5 ton was applied to oxide powder with Pt mesh (80 meshes) simultaneously to form a pellet (10 mm × 10 mm × 1 mm) so that Pt mesh electrodes could be embedded inside the oxide as shown in Figure 3. Both Pt mesh electrodes were kept from contacting each other and being exposed at the surface of the pellet. Pressed pellets were sintered in air at 1000 °C for 6 h in order to reduce grain boundaries and minimize the influence of grain-to-grain contacts. After cooling, 3.0 mg carbon was loaded at the pellet surface and heated to 700 °C in air at 10 °C min^{-1}. A voltmeter and an ampere meter measured voltage and current respectively. In these measurements, the carbon-loaded side was designated to be an anode side.

Results and Discussion

Catalyst Characterization. X-ray diffractograms of the oxides after thermal aging (800 °C, 24 h in air) are shown in Figure 4. Only a single phase corresponding to the cubic-type structure was observed in all oxides. Y^{3+} ion and Nd^{3+} ion were incorporated into ZrO_2 cubic structure, and Zr^{4+} ion were incorporated into CeO_2 cubic structure.

The crystalline diameters calculated from the Scherrer equation and BET surface areas of the oxides are shown in Table 1. Crystalline diameters in the fresh condition are almost 10 nm for all oxides. After thermal aging (800 °C, 24 h in air), ZrYO showed significant increase in the diameter to 47 nm, whereas ZrNdO and CeZrO maintained small crystal sizes, 15 and 10 nm respectively. The similar trend in thermal stability was indicated in BET surfaces. The surface areas in all oxides were above 80 $m^2 g^{-1}$ in the fresh condition. Only ZrYO decreased to below 10 $m^2 g^{-1}$ after thermal aging.

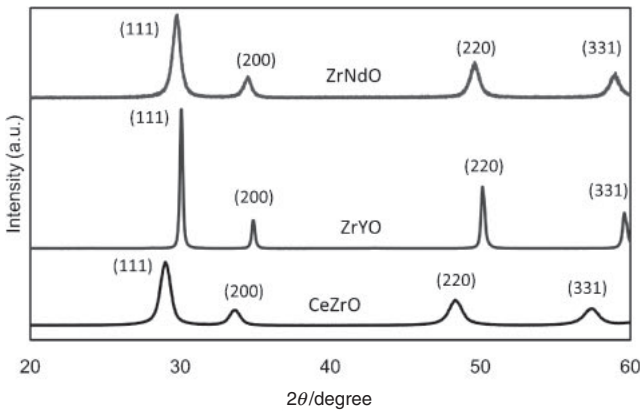

Figure 4. X-ray diffractograms of the oxides after thermal aging (800 °C, 24 h in air).

Table 1. BET Surfaces and Crystalline Diameters of Oxides

	BET surface area/$m^2 g^{-1}$		Crystalline diameter/nm	
	Fresh	Aged[a)]	Fresh	Aged[a)]
$Zr_{0.8}Y_{0.2}O_{2-X}$	118	7	9	47
$Zr_{0.7}Nd_{0.3}O_{2-X}$	104	61	11	15
$Ce_{0.7}Zr_{0.3}O_{2-X}$	86	65	8	10

a) Aged: 800 °C, 24 h in air.

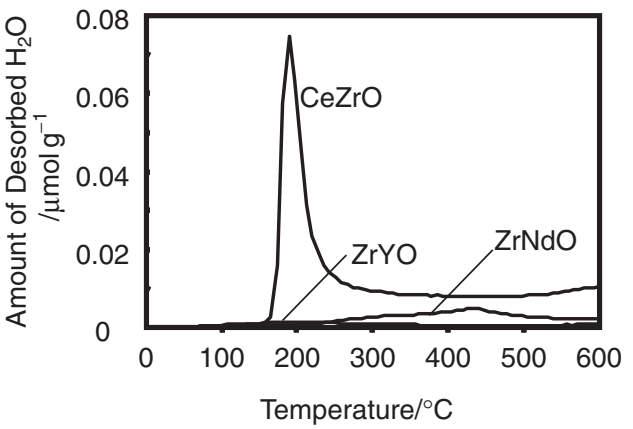

Figure 5. Oxygen release properties of the Pt-loaded oxides in 2% H_2/He. Pretreatment condition: 10% O_2 in He, R.T. to 600 °C. Catalyst condition: aged at 800 °C for 24 h in air.

The redox properties of the catalysts after thermal aging (800 °C, 24 h in air) were studied by the H_2-TPR, and the desorbed H_2O profiles are shown in Figure 5. Only CeZrO showed an apparent large peak of desorption at around 200 °C. This peak can be interpreted as oxygen desorption that is related to Pt.[20] Table 2 shows the total amount of released oxygen determined from the amount of desorbed H_2O in the observed temperature range. ZrYO showed around one fifteenth part and ZrNdO showed around one fifth part of the oxygen release amount compared to that of CeZrO, which indicated that ZrYO and ZrNdO had inferior OSC properties relative to CeZrO.

Catalytic Carbon Oxidation Activity in TG/DTA. Figure 6a shows profiles of the carbon oxidation rates in the loose contact condition of catalyst–carbon mixtures with

Table 2. Total Amount of Released Oxygen in 2% H_2/He in the Range of R.T. to 600 °C

	ZrYO	ZrNdO	CeZrO
Amount of released oxygen/mmol g^{-1}	0.010	0.029	0.14

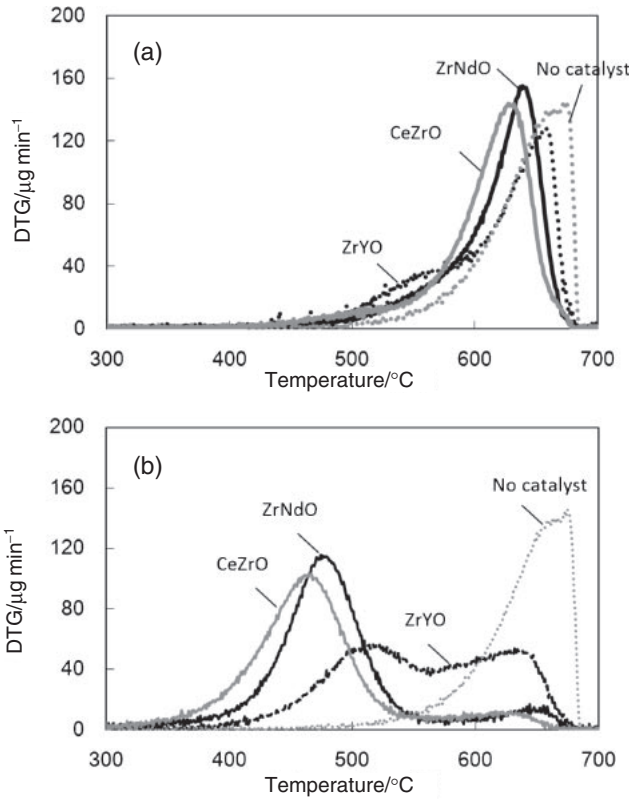

Figure 6. Carbon oxidation of the Pt-loaded oxides by O_2 after thermal aging (800 °C, 24 h in air) under (a) loose contact condition and (b) tight contact condition in TG-DTA.

temperature. The catalysts were thermally aged at 800 °C for 24 h in air. ZrYO, ZrNdO, and CeZrO lowered carbon-oxidation onset temperatures by around 50 °C and temperatures corresponding to DTG peaks by around 10 to 50 °C compared with carbon only. In addition, such catalytic effect was sustained even at a higher temperature around 600 °C in which noncatalytic carbon oxidation was facilitated. In comparison among the three catalysts, CeZrO lowered the temperature corresponding to the DTG peak the most, followed by ZrNdO with only a slight difference. Oxidation rates of ZrNdO and CeZrO in a lower temperature range around 450 to 580 °C were quite similar, whereas ZrYO showed slightly higher oxidation rates than the others in the same temperature range.

Figure 6b shows the profiles in the tight contact condition with temperature. The carbon-oxidation onset temperatures and DTG peaks of the catalysts shifted significantly to a lower temperature compared with those in the loose contact condition. This result indicated sufficient contact between catalyst and carbon accelerated the carbon oxidation, consistent with reported literature.[15,16,21] CeZrO showed a single peak at around 480 °C, which was slightly lower than that of ZrNdO. On the other hand, ZrYO showed a double peak in the higher temperature range around 500 and 630 °C, thus ZrYO showed inferior oxidation activity to the others. ZrYO has substantially smaller surface area after thermal aging compared to the others as shown in Table 1 which presumably results in insufficient contact with carbon even under the tight contact as in accordance with the literature.[15,22] The first peak at around 500 °C may indicate intrinsic activity of ZrYO. The insufficient contact with carbon led to slower carbon oxidation at around 500 °C and the residual carbon was oxidized at a higher temperature of about 630 °C. Based on these results, CeZrO and ZrNdO showed good potential to oxidize the carbon; meanwhile ZrYO was inferior to the other catalysts. Under the catalyst–carbon mixture condition, the surface areas of the catalysts were likely to influence the carbon oxidation performance.

Carbon Oxidation Activity of the Catalyst Loaded on DPF. Catalytic carbon oxidation was studied under the actual contact condition between carbon and catalyst on the DPF substrate. CO_2 concentrations resulted from carbon oxidation are shown in Figure 7. In the fresh condition and aged conditions, CO_2 generation started at around 400 °C indicating the onset of carbon-oxidation. In the fresh condition, as shown in Figure 7a, there was little difference in CO_2 concentrations among the catalysts. On the contrary, ZrNdO and ZrYO showed higher concentrations than that of CeZrO after 800 °C aging and 1000 °C aging as in Figures 7b and 7c, respectively. Table 3 shows CO_2 concentrations at 590 °C (typical real world DPF regeneration condition). CO_2 concentrations for ZrNdO and ZrYO in aged condition were similar to those observed in the fresh condition. ZrYO showed good carbon oxidation activity considering its smaller surface area after thermal aging. On the contrary, CeZrO showed inferior oxidation activity, which was different from the results of TG-DTA measurement. The influence of the surface area on carbon oxidation activity seems smaller, unlike the mixture conditions of catalyst and carbon. The carbon contacts around the catalyst particles under the mixture condition of catalyst and carbon, whereas the carbon contacts on the surface of the catalyst layer when the catalyst are coated on the DPF substrate. Therefore, it is assumed that the contact area to carbon is relatively constant for the coated catalysts on the DPF substrate and less subject to difference in surface areas of the catalysts.

As shown in Table 2, the OSC properties for ZrYO and ZrNdO were much smaller than that of CeZrO. Aneggi et al. explained the soot oxidation activity for CeZrO (Ce-rich type) was related to oxygen storage capacity and surface area.[22] In the condition insusceptible to the surface areas of the catalysts, it is not possible to explain the higher activities for ZrYO and ZrNdO based on the OSC properties.

Isotopic Tracer Measurement. In order to discuss the promoting scheme of carbon oxidation for ZrYO and ZrNdO, oxygen isotope was used as a tracer to identify the oxygen source in the carbon oxidation. Figure 8 shows concentrations of CO_2, CO, and O_2 species monitored downstream of the mixtures of carbon and catalysts (aged at 800 °C for 24 h in air), and carbon only, in oxygen isotope atmosphere (3.5% $^{18}O_2$ in He) at 600 °C. After introducing oxygen isotope $^{18}O_2$, $^{18}O_2$ decreased to almost zero in both catalyzed reaction and

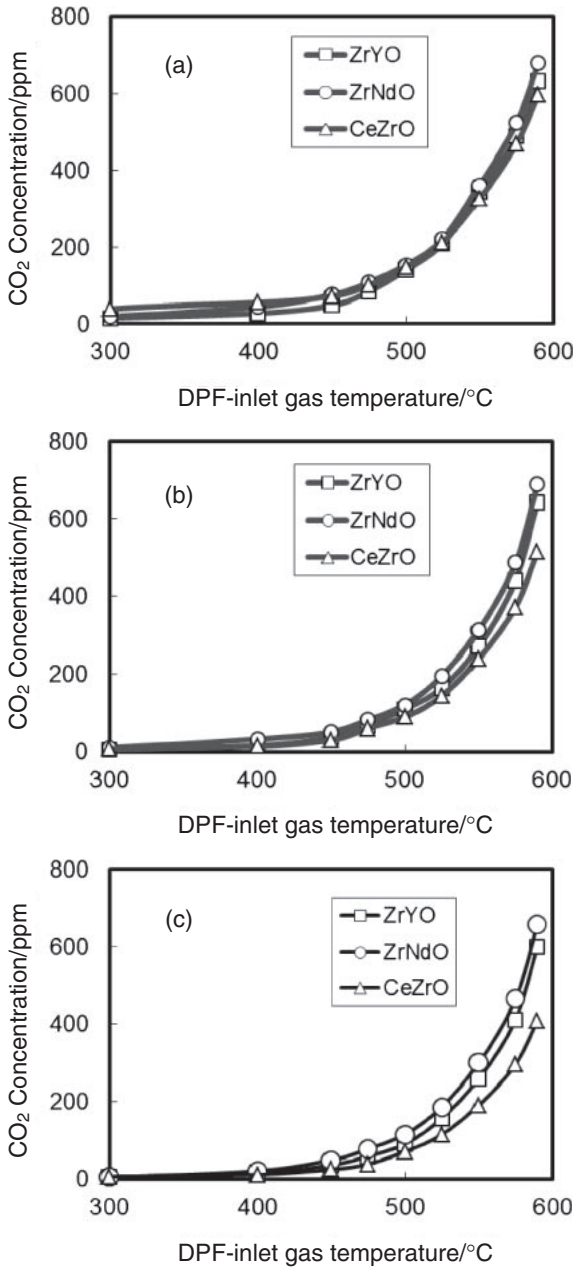

Figure 7. Carbon oxidation of the Pt-loaded oxides under the condition of the catalysts coated on DPF substrate. Catalyst condition: (a) fresh, (b) aged at 800 °C for 24 h in air, and (c) aged at 1000 °C for 24 h in air.

Table 3. CO_2 Concentrations at 590 °C in Temperature Ramp Experiments

	CO_2 concentration/ppm		
	ZrYO	ZrNdO	CeZrO
Fresh	630	677	597
800 °C, 24 h	642	688	514
1000 °C, 24 h	601	657	409

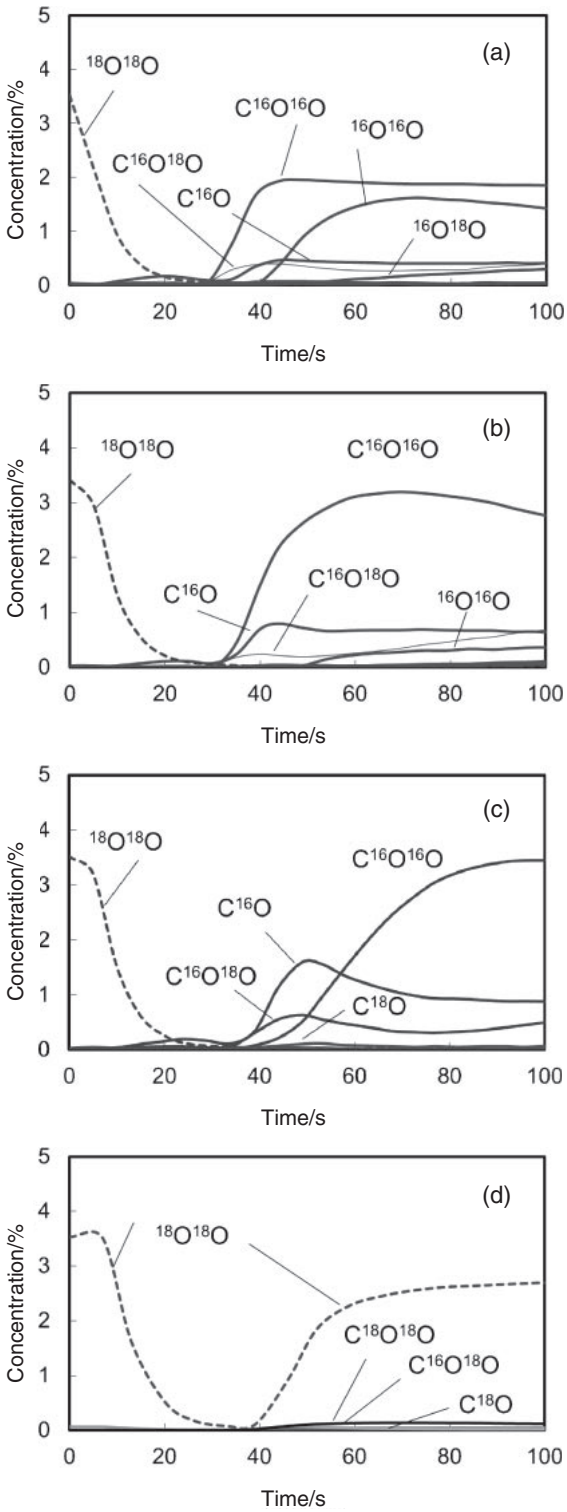

Figure 8. Generation of CO, CO_2, and O_2 species in carbon oxidation after $^{18}O_2$ introduction for Pt-loaded oxides, (a) ZrYO, (b) ZrNdO, (c) CeZrO, and (d) carbon only (without adding catalyst). Catalyst condition: aged at 800 °C for 24 h in air.

noncatalyzed reaction because it took a little time to exchange the atmosphere in the quartz tube filled with He by $^{18}O_2$ in He.

$^{18}O_2$ concentration for carbon only increased from around 40 s while the concentrations for all catalysts were kept at zero, which indicated $^{18}O_2$ was stored by the catalysts. CO_2

Table 4. Total Amount of ^{16}O Released from Catalysts and Used for Carbon Oxidation in 100 s

	Released ^{16}O /mmol-O g^{-1}	Used ^{16}O for carbon oxidation/mmol-O g^{-1}
ZrYO	8.7	4.9
ZrNdO	8.5	8.1
CeZrO	6.9	6.9
Carbon only	0	0.1

concentration was quite low in the noncatalyzed reaction as shown in Figure 8d, and the evolved $C^{18}O$ and $C^{18}O_2$ were attributed to the reaction between carbon and gas-phase oxygen. On the contrary, $C^{16}O$, $C^{16}O^{16}O$, and $C^{16}O^{18}O$ evolved in the catalyzed reaction as shown in Figures 8a–8c, and those concentrations were much higher than CO and CO_2 in the noncatalyzed reaction. Since gas phase is filled with $^{18}O_2$ in He, generation of $C^{16}O$, $C^{16}O^{16}O$, and $C^{16}O^{18}O$ containing ^{16}O indicates the usage of released lattice oxygen in the catalysts. It was indicated the lattice oxygen had higher carbon oxidizing activity than gas-phase oxygen.

For any catalysts, $C^{16}O^{16}O$ was observed at around 30 s after introducing oxygen isotope, then, its concentration suddenly increased up to around 3.5% in 80 s for ZrNdO and CeZrO. ZrYO shows lower $C^{16}O^{16}O$ concentration than the others, whereas $^{16}O^{16}O$ concentration was higher than the others instead.

Table 4 shows total amounts of evolved ^{16}O and consumed ^{16}O in the catalytic oxidation in 100 s determined from the results shown in Figure 8. ZrYO and ZrNdO evolved the active lattice oxygen more efficiently than that of CeZrO. However, the consumed ^{16}O for ZrYO was lower than ZrNdO and CeZrO, which indicated ZrYO evolved more oxygen without being used for the carbon oxidation than those of ZrNdO and CeZrO. A possible reason why the evolved active oxygen hardly contributed to the carbon oxidation may be related to the poor contact condition between carbon and the catalyst as mentioned in the TG-DTA measurement result.

^{16}O was consumed in the noncatalyzed carbon oxidation in $^{18}O_2$/He atmosphere though the amount was much lower than that of catalyzed carbon oxidation. The reaction between ^{16}O and carbon can be attributed to ^{16}O originally existing as surface carbon–oxygen complex on the carbon.[15]

Oxygen exchange reaction of the catalysts under carbon-free condition in oxidizing atmosphere was studied. Figure 9 shows concentrations of O_2 species monitored downstream of the catalysts (aged at 800 °C for 24 h in air) in oxygen isotope atmosphere at 600 °C. Three types of oxygen were observed, $^{16}O^{16}O$, $^{16}O^{18}O$, and $^{18}O^{18}O$. As similar to isotopic tracer method in carbon oxidation, gas phase was filled with oxygen isotope $^{18}O_2$ in He. Therefore, for all catalysts, it can be explained that lattice oxygen (^{16}O) was evolved as $^{16}O^{16}O$ or $^{16}O^{18}O$ and gas-phase oxygen (^{18}O) was stored in the catalysts by the oxygen exchange reaction. After the oxygen isotope introduced, about 90, 75, and 65% of $^{18}O^{18}O$ were replaced by $^{16}O^{16}O$ for ZrYO, ZrNdO, and CeZrO respectively within 100 s. ZrYO showed the highest capability to evolve the lattice oxygen; whereas CeZrO was the lowest. The order of the capability of oxygen exchange in the oxidizing condition among the catalysts was contrary to that of oxygen release properties in the reductive condition mentioned above. The higher oxygen exchange properties of ZrYO and ZrNdO could explain the superior carbon oxidation performances compared to CeZrO as shown in Table 3.

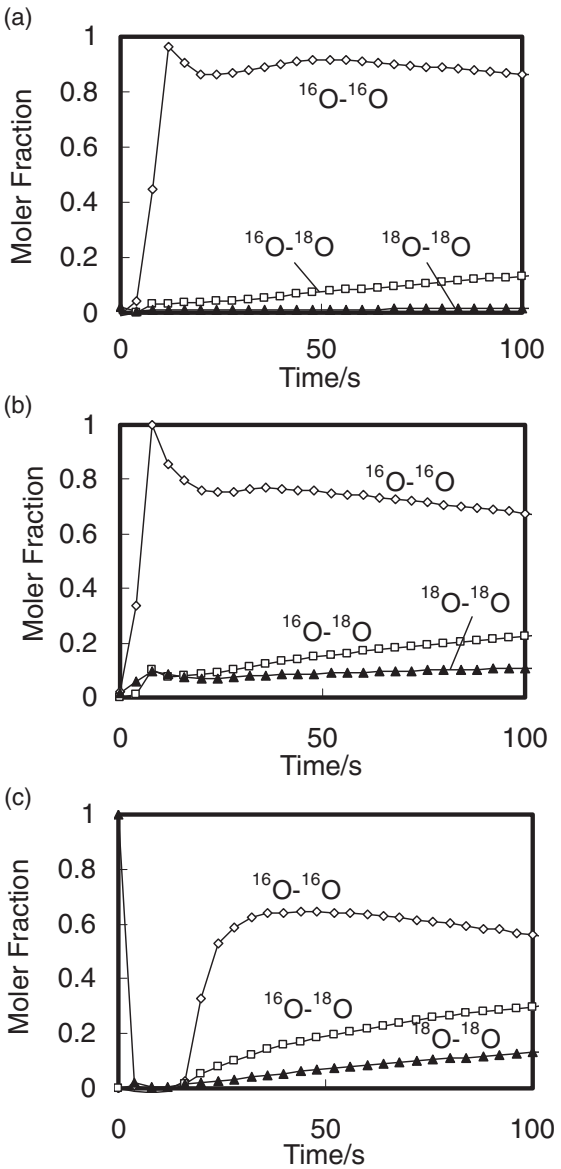

Figure 9. Generation of O_2 species with oxygen exchange reaction of the Pt-loaded oxides after $^{18}O_2$ introduction for (a) ZrYO, (b) ZrNdO, and (c) CeZrO. Catalyst condition: aged at 800 °C for 24 h in air.

In order to discuss the oxygen exchange scheme, the reaction equations for Zr-based oxide and Ce-based oxide are shown below. In order to explain the reaction simply, ZrO_2 and CeO_2 are employed as representatives in the equations, 1a with 1b and 2a with 2b, respectively.

$$Zr^{4+}O^{2-}{}_2 \rightarrow O_2 + Zr^{4+}Vo''{}_2 + 4e^- \quad (1a)$$

$$O_2 + 4e^- + Zr^{4+}Vo''{}_2 \rightarrow Zr^{4+}O^{2-}{}_2 \quad (1b)$$

$$4Ce^{4+}O^{2-}{}_2 \rightarrow 2Ce^{3+}{}_2O^{2-}{}_3 + O_2 + Vo'' \quad (2a)$$

$$2Ce^{3+}{}_2O^{2-}{}_3 + Vo'' + O_2 \rightarrow 4Ce^{4+}O^{2-}{}_2 \quad (2b)$$

Zr-Based oxides evolve lattice oxygen accompanied by electron generation as shown in eq 1a. The gas-phase oxygen is stored into the oxide with electron as shown in eq 1b. For the oxygen exchange reaction, the reactions indicated by eqs 1a and 1b occur simultaneously. In the oxygen release reaction (eq 1a), oxygen defect is also generated at the surface of the oxides. The electric conductivities for ZrYO and ZrNdO are about 150-times and 40-times as high as that for CeO_2 having relatively higher conductivity than CeZrO at 600 °C.[23] The electric conductivity consists of components for oxide ion and electron. ZrYO and ZrNdO contain no elements generating the valence change, thus the ratio of oxide ion conductivity in the electric conductivity could be much higher than that for CeZrO. Therefore, oxide ion conductivities for ZrYO and ZrNdO are higher than that for CeZrO. Because of the high oxide ion mobility, the lattice oxygen can easily transfer to the oxygen defect for Zr-based oxides. Therefore it is assumed that the density of lattice oxygen at the surface is kept high enough to continue the oxygen exchange reaction. In other words, oxygen existing both at the surface and in the bulk may possibly be used for the oxygen exchange.

Ce-Based oxides can behave with different schemes shown in eqs 2a and 2b. Since the valence energies of Ce ion at the valence 4+ in CeO_2 and 3+ in Ce_2O_3 are very close to each other, the Ce ion easily changes its valence depending on the atmosphere. This property can be just as valid for the oxygen exchange reaction. As shown in the eq 2a, the lattice oxygen is released without generating electron and the valence state of Ce ion changes from 4+ to 3+. In the oxygen storage scheme shown in eq 2b, the valence state of Ce ion changes from 3+ to 4+ adversely and electron supplied from Ce ion is utilized for the oxygen molecular dissociation. Because the Ce ion in 3+ and 4+ are very stable in the oxide, the motive force of oxide ion could not be obtained.

Electrochemical Measurement. As mentioned in previous section, ZrYO and ZrNdO are assumed to generate the electron and transfer the lattice oxygen in the oxygen exchange reaction. Therefore, if the oxygen exchange reaction plays an important role in promoting the carbon oxidation, a similar framework could be adopted for the carbon oxidation. Equations 3a and 3b indicate a scheme of carbon oxidation by lattice oxygen and a scheme of oxygen storage into the lattice, respectively. In order to verify this assumption, the behavior of electron at the moment of carbon oxidation was first investigated by measuring the current generated in the oxide. In this measurement, both Pt-loaded sample and Pt-free sample were studied.

Figure 10 shows measured current generated during carbon oxidation for each Pt-free oxide. Since the anode of this experiment was designated at the carbon-loaded side, generated negative current value indicated electron generated at carbon-loaded side and circulated to the opposite side of the pellet. For ZrYO and ZrNdO, apparent negative peak at around 500 to 600 °C was observed and the current value decreased to zero around when the carbon oxidation completed, which indicated that the electron generation could be related to the carbon oxidation.

Feasible behaviors of electron for ZrYO and ZrNdO indicated from the measurement results are schematically shown in Figure 11. As the only electron source is in the oxide

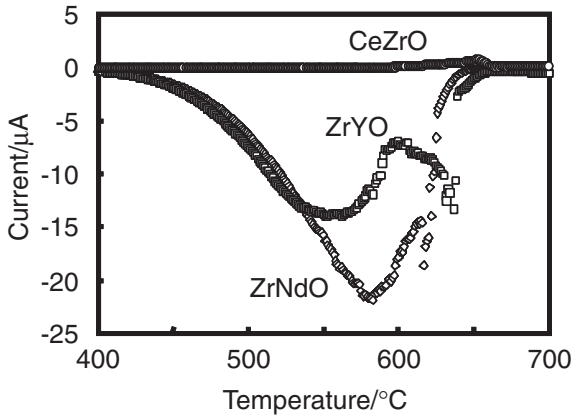

Figure 10. Temperature dependence of the generated electron by carbon oxidation in each Pt-free oxide.

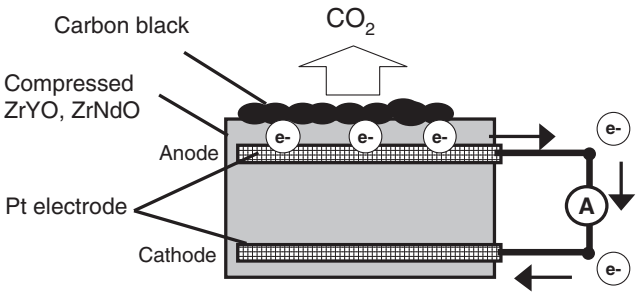

Figure 11. Schematic model of the electron generation caused by carbon oxidation.

for this reaction system, the negative current indicates that the lattice oxygen reacted with carbon in association with the electron generation as in eq 3a. In addition, negative current was observed during the entire time of carbon oxidation, which could explain that consumption and replenishment of the lattice oxygen occurred simultaneously.

$$C + 2O^{x}o \rightarrow CO_2 + 4e^{-} \quad (3a)$$

$$O_2 + 4e^{-} \rightarrow 2O^{x}o \quad (3b)$$

Current was not observed for CeZrO over the entire temperature range indicating that none of the electron was generated during the carbon oxidation. As discussed above, this behavior suggests that CeZrO should not evolve the lattice oxygen with electron generation but with the valence change of Ce ion.

Figure 12 shows measured current generated in carbon oxidation for each Pt-loaded oxides. The magnitudes of current for ZrYO and ZrNdO decreased compared with those for Pt-free oxides as shown in Figure 10. This result indicates that Pt loading decreased the magnitude of the charge-up state of the surface. Presumably, it is due to promoting the electron diffusion in the oxide by variable range hopping between Pt sites.

On the other hand, current was not observed for Pt-loaded CeZrO as in the case of Pt-free CeZrO, indicating that Pt loading never changed its electron state in the carbon oxidation reaction.

For the next step to discuss a behavior of lattice oxygen, electromotive force during carbon oxidation was observed.

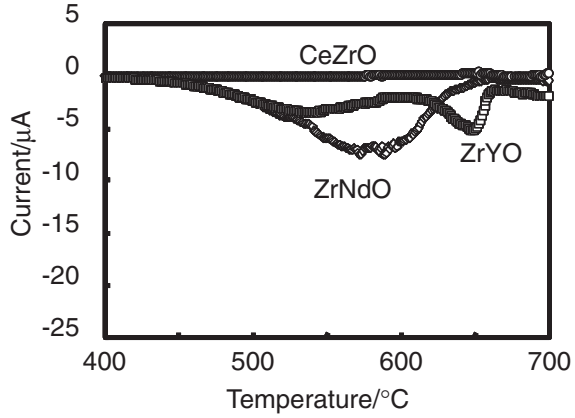

Figure 12. Temperature dependence of the generated electron by carbon oxidation in each Pt-loaded oxide.

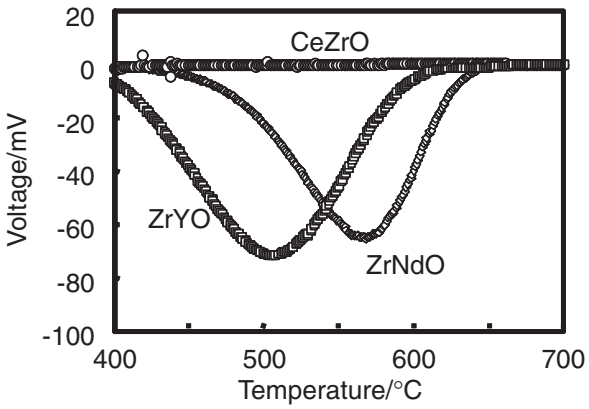

Figure 13. Temperature dependence of the electromotive force generated by carbon oxidation in each Pt-free oxide.

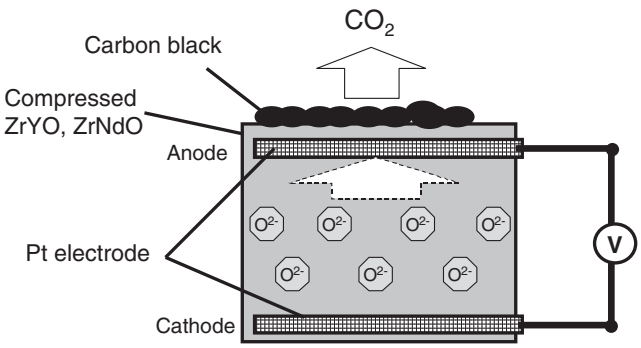

Figure 14. Schematic model of the electromotive force caused by carbon oxidation.

Figure 13 shows the measured electromotive force generated in each Pt-free oxide. As schematically shown in Figure 14, the generated electromotive force is mainly attributed to electric unbalance by the biased population of the oxide ion, which is well known as Nernst relation in oxide ion conductors. Since anode was designated at a carbon-loaded side, negative value indicated that oxide ion moved to the carbon-loaded side. ZrYO and ZrNdO showed apparent negative peak structure during the carbon oxidation. It means that lattice oxygen was continuously supplied to the carbon-loaded surface from bulk of ZrYO or ZrNdO during the carbon oxidation. In other words, the carbon-loaded surface can easily access the lattice oxygen due to the supply of oxygen from the oxide bulk. This result supports the possibility that ZrYO and ZrNdO could promote carbon oxidation with bulk oxygen as well as the results in the isotopic tracer measurement in the previous section.

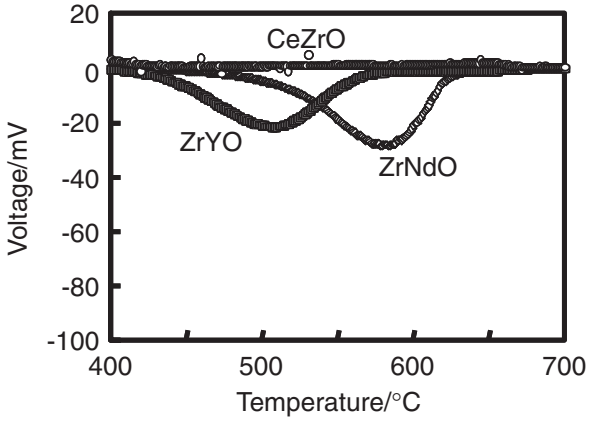

Figure 15. Temperature dependence of the electromotive force generated by carbon oxidation in each Pt-loaded oxide.

This specific phenomenon of ZrNdO and ZrYO may be also related to their catalytic properties after the thermal aging as shown in Figure 7 and Table 3. The transfer of bulk lattice oxygen to the surface should be affected by grain boundary in the oxide. As shown in Table 1, thermal aging could grow the crystalline diameter while decreasing the grain boundary. Therefore, it is expected that the mobility of lattice oxygen may be enhanced by the thermal treatment. Consequently, carbon oxidation of ZrYO and ZrNdO can be sustained even after the thermal aging treatment.

On the other hand, CeZrO never generated electromotive force during the carbon oxidation. It was indicated that an electric unbalance was barely observed for CeZrO during the carbon oxidation and lattice oxygen of the oxide bulk may hardly be used.

In the case of Pt-loaded oxide, similar behaviors to Pt-free oxide were observed although the magnitudes of the electromotive force were decreased as shown in Figure 15. Presumably, promotion of electronic conductivity by Pt loading is responsible for the decreasing electromotive force of ZrYO and ZrNdO.

ZrYO showed negative peak at comparative temperature to ZrNdO both in the current measurement and electromotive force observation during carbon oxidation, in spite of its smaller surface area than ZrNdO. As the pelletized oxides were used in this measurement, the surface area was unlikely to influence the catalytic properties as well as the carbon oxidation activity tests using DPF substrate.

PM Oxidation Promotion Model for ZrYO and ZrNdO. Carbon oxidation schemes in ZrYO, ZrNdO, and CeZrO were discussed as follows. A feasible reaction model for ZrYO and ZrNdO is compared with that for CeZrO as schematically shown in Figure 16. As depicted in the isotopic tracer measurement during carbon oxidation, supplying of lattice oxygen to the carbon plays a crucial role in promoting the

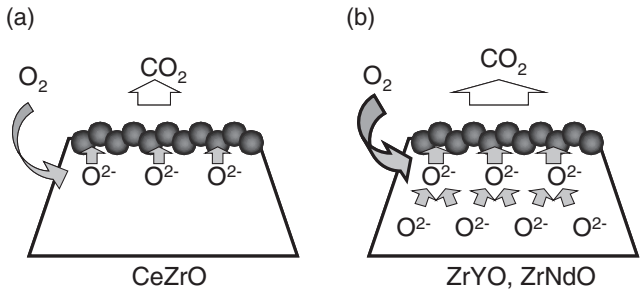

Figure 16. Schematic model of the promoting scheme of carbon oxidation in each oxide.

catalytic oxidation. The lattice oxygen, O^{2-}, is assumed to change into the different active oxygen species at the surface of the oxide and oxidize the carbon efficiently.

In the case of CeZrO, it was speculated by the isotopic tracer measurement and electrochemical measurement that the lattice oxygen at the surface was mainly used in the carbon oxidation with the oxygen exchange reaction as shown in Figure 16a. As only lattice oxygen at the surface of the oxide contributes to the carbon oxidation, the amount of supplied lattice oxygen to the carbon can run short in comparison with that for ZrYO or ZrNdO.

ZrYO and ZrNdO might have an advantage to promote the oxygen exchange reaction in the carbon oxidation. As shown in Figure 16b, consuming oxide ion (lattice oxygen) in the carbon oxidation generates the oxygen defect that is close to a carbon-loaded site, and different oxide ion diffuses to the oxygen defect. This behavior can be attributed to high oxide ion conductivity and helps provide a continuous supply of lattice oxygen from the oxide bulk to carbon. On the other hand, the electron was left in the oxide in the carbon oxidation (eq 3a), and the electron enhances the dissociation of oxygen molecular into the oxide ion.

Moreover, it is well known that the Pt could reduce the dissociation energy of adsorbed oxygen molecule.[24,25] Therefore, for the Pt-loaded oxides, the facilitation of both the electron diffusion and oxygen dissociation by Pt may contribute to promote the oxygen storage reaction, which leads to enhancing the carbon oxidation.

Conclusion

ZrYO and ZrNdO indicated higher carbon oxidation activity than that of CeZrO under the condition of a Pt-loaded oxide coated on a DPF substrate. ZrYO and ZrNdO were found to have poor oxygen storage capacity in H_2-TPR method but enhance oxygen exchange reaction in oxidizing atmosphere in the isotopic tracer method. Those oxides released lattice oxygen that can promote the carbon oxidation as an active oxygen species more effectively than that of CeZrO. Electrochemical measurements were performed to theorize the behavior of electron and lattice oxygen during carbon oxidation reaction. Electron generation was observed, and electromotive force indicating biased population of oxide ion was generated during the carbon oxidation for ZrYO and ZrNdO. These results indicate the reaction scheme consisting of the dissociation of oxygen molecule into an oxide ion by an electron and carbon oxidation by the oxide ion for ZrYO and ZrNdO.

References

1 B. A. A. L. van Setten, M. Makkee, J. A. Moulijn, *Catal. Rev.* **2001**, *43*, 489.
2 C. M. Somers, B. E. McCarry, F. Malek, J. S. Quinn, *Science* **2004**, *304*, 1008.
3 R. Allanson, P. G. Blaeman, B. J. Cooper, H. Hess, P. J. Silcock, A. P. Walker, SAE Paper, **2002**, 2002-01-0428.
4 B. L. Edgar, K. Balakrishnan, X. Zhou, M. D. Rumminger, SAE paper, **2001**, 2001-01-1342.
5 B. J. Cooper, J. E. Thoss, SAE Paper, **1989**, No. 890404.
6 J. Oi-Uchisawa, A. Obuchi, A. Ogata, R. Enomoto, S. Kushiyama, *Appl. Catal., B* **1999**, *21*, 9.
7 A. Setiabudi, M. Makkee, J. A. Moulijn, *Appl. Catal., B* **2004**, *50*, 185.
8 K. Krishna, M. Makkee, *Catal. Today* **2006**, *114*, 48.
9 J. C. Summers, S. Van Houtte, D. Psaras, *Appl. Catal., B* **1996**, *10*, 139.
10 J. Lahaye, S. Boehm, Ph. Chambrion, P. Ehrburger, *Combust. Flame* **1996**, *104*, 199.
11 A. Setiabudi, J. Chen, G. Mul, M. Makkee, J. A. Moulijn, *Appl. Catal., B* **2004**, *51*, 9.
12 K. Harada, Y. Tsushio, A. Takami, *J. Jpn. Pet. Inst.* **2005**, *48*, 216.
13 A. Takami, K. Harada, Y. Tsushio, *J. Jpn. Pet. Inst.* **2007**, *50*, 102.
14 K. Harada, Y. Tsushio, A. Takami, *Science and Technology in Catalysis*, Kodansha/Elsevier, Tokyo, **2007**, p. 601.
15 A. Bueno-López, K. Krishna, M. Makkee, J. A. Moulijn, *J. Catal.* **2005**, *230*, 237.
16 K. Krishna, A. Bueno-López, M. Makkee, J. A. Moulijn, *Appl. Catal., B* **2007**, *75*, 189.
17 J. Au-Yeung, A. T. Bell, E. Iglesia, *J. Catal.* **1999**, *185*, 213.
18 D. Fei, A. Suda, T. Tanabe, JP. Unexamined Patent, **2005**, 2005-9884.
19 M. Haneda, T. Mizushima, N. Kakuta, A. Ueno, *Nippon Kagaku Kaishi* **1997**, *3*, 169.
20 A. Trovarelli, *Catalysis by Ceria and Related Materials*, Imperial College Press, London, **2002**, p. 101.
21 M. A. Małecka, L. Kępiński, W. Miśta, *Appl. Catal., B* **2007**, *74*, 290.
22 E. Aneggi, C. de Leitenburg, G. Dolcetti, A. Trovarelli, *Catal. Today* **2006**, *114*, 40.
23 K. Harada, H. Yamada, K. Okamoto, A. Takami, *Catal. Surv. Asia* **2010**, *14*, 176.
24 T. Zambelli, J. V. Barth, J. Wintterlin, G. Ertl, *Nature* **1997**, *390*, 495.
25 P. Gambardella, Ž. Šljivančanin, B. Hammer, M. Blanc, K. Kuhnke, K. Kern, *Phys. Rev. Lett.* **2001**, *87*, 056103.